A Metamaterial-Driven Approach for Improved Performance of Fatigue Crack Detection by Amplifying Nonlinear Ultrasonic Features

Yiran Tian, Haoyu Fu, and Yanfeng Shen*
University of Michigan-Shanghai Jiao Tong University Joint Institute, Shanghai Jiao Tong University, Shanghai, 200240, China

ABSTRACT

Ultrasonic guided waves have emerged as a powerful tool in nondestructive testing, demonstrating exceptional potential for structural damage assessment due to their distinct advantages in long-range propagation and high sensitivity to a variety of damage types. Conventional linear ultrasonic methods predominantly identify macroscopic defects, whereas nonlinear ultrasonic techniques exhibit superior sensitivity to incipient fatigue crack formation, attracting growing research interest within Structural Health Monitoring (SHM) and Nondestructive Evaluation (NDE) communities. However, practical implementation faces critical limitations arising from weak nonlinear signatures and low signal-to-noise ratios associated with incipient cracks in large-scale engineering structures. To address these challenges, this study proposes a metamaterial-enhanced methodology that substantially amplifies second harmonic signal amplitude, thereby improving fatigue crack detection sensitivity. A metamaterial-assisted wave modulation device, i.e., defect mode metamaterial (DMM), is engineered through strategic implementation of a pillar-type metamaterial array containing an artificial defect cavity formed by dual resonator removal. This configuration establishes a localized resonant cavity that concentrates wave energy distribution, particularly enhancing second harmonic components, while a circular piezoelectric transducer attached facilitates effective signal acquisition. Numerical simulations demonstrate the system's capability to amplify weak second harmonic signals generated by micro-scale fatigue cracks under sustained cyclic loading conditions. The observed energy localization mechanism, achieved through DMM design, effectively overcomes conventional limitations in nonlinear ultrasonic detection sensitivity. This metamaterial-enabled approach to elastic wave manipulation opens up new possibilities for improving the sensitivity of nonlinear ultrasonic techniques in practical SHM/NDE applications.

Keywords: Elastic metamaterial; Defect mode; Fatigue crack; Nonlinear ultrasonics; Structural health monitoring

1. INTRODUCTION

Fatigue-induced fractures pose a critical threat to structural integrity in engineering systems, driven by their complex initiation mechanisms and difficulties in early-stage detection[1]. These fractures evolve from microscopic precursors—material dislocations or subcritical microcracks—under cyclic loading, progressing unpredictably to critical dimensions that precipitate catastrophic failures[2]. This underscores the necessity for proactive assessment of cumulative damage evolution to ensure operational reliability. While ultrasonic methods have become indispensable in Nondestructive Evaluation (NDE) and Structural Health Monitoring (SHM), conventional linear approaches relying on wave reflection, absorption, and mode conversion exhibit insufficient sensitivity to incipient cracks, detecting defects only at macroscale dimensions[3,4]. Nonlinear ultrasonic techniques, exploiting higher-harmonic generation (HHG), subharmonic emission, and wave modulation phenomena[5-7], demonstrate superior capability in identifying nascent damage, including fatigue cracks, delamination, microstructural changes, bolted joint loosening, and impact damage in composites[8-10]. A key aspect of nonlinear detection involves analyzing the amplitude variations of higher-order harmonics due to cumulative effects[11].

Current research predominantly correlates crack severity with contact acoustic nonlinearity (CAN) and second harmonic amplitudes. Sampath et al. developed a nonlinear ultrasonic three-wave mixing technique for accurately detecting and localizing early-stage fatigue cracks[12]. Lim et al. presented a comprehensive noncontact visualization technique for fatigue cracks based on nonlinear ultrasonic wave modulation[13]. Despite these advancements, early detection and

* Corresponding authors
Email address: yanfeng.shen@sjtu.edu.cn

Health Monitoring of Structural and Biological Systems XIX, edited by Zhongqing Su, Kara J. Peters
Fabrizio Ricci, Piervincenzo Rizzo, Proc. of SPIE Vol. 13437, 134370G
 · 0277-786X · doi: 10.1117/12.3051044

continuous monitoring of fatigue cracks remain challenging[14], particularly due to the faint nonlinear features during initial crack nucleation and limitations in sensitivity and signal-to-noise ratios in large-scale structures[15], highlighting the imperative to amplify subtle nonlinear features.

Acoustic/elastic metamaterials and phononic crystals (PnCs) have emerged as promising tools for wave manipulation[16], enabling unprecedented control over wave focusing, refraction, filtering, steering, and energy harvesting[17-20]. Recent metamaterial-based sensing architectures demonstrate enhanced acoustic signal resolution. Chen et al. developed a metamaterial-enhanced acoustic sensing system achieving over 20 dB signal-to-noise enhancement through strong wave compression effects[21]. Huang et al. introduced a trumpet-shaped acoustic metamaterial that significantly enhances sound wave selection for detecting rotating machinery faults[22]. Xiao et al. proposed a structural enhancement approach for diagnosing faults in rotating machinery through line-defect PnC sensing[23]. Despite these advancements, extending such principles to elastic mechanical waves presents substantial challenges due to their higher degrees of freedom.

Incorporating defects into PnCs has gained attention in piezoelectric energy harvesting (PEH), leveraging energy localization and amplification near defect cavities. Zhang et al. utilized PnCs to enhance the electrical output performance of PEH devices while broadening their energy harvesting frequency range[24]. Jo et al. proposed a PnC with triple defects arranged in an L-shape for broadband PEH applications[25]. Lee et al. explored high-performance PEH at multiband frequencies using periodically arranged trampoline metamaterials[26]. Ma et al. engineered elastic metamaterial cavities with multiple modes to harvest flexural wave energy, achieved through the drilling of periodic holes in thin aluminum plates[27]. However, leveraging these principles to enhance nonlinear ultrasonic interrogation through direct wavefield manipulation remains unexplored, particularly for fatigue-related nonlinear feature extraction.

This study introduces a metamaterial-assisted wave modulation paradigm to amplify nonlinear ultrasonic signatures, with a focus on second harmonic signal enhancement. A pillared metamaterial array is first analyzed for its bandgap characteristics, followed by the strategic removal of two resonators to create a defect-localized cavity. This engineered configuration concentrates wave energy intensity within the cavity region, preferentially amplifying second harmonic components. A centrally positioned piezoelectric transducer captures the enhanced signals, with numerical simulations benchmarking performance against conventional smooth plates. By synergizing defect mode metamaterials (DMM) with nonlinear ultrasonics, this work establishes a framework for sensitive fatigue crack monitoring. The demonstrated harmonic amplification mechanism addresses sensitivity limitations in SHM/NDE, enabling earlier detection of critical damage precursors within industrial-scale implementations.

2. DESIGN STRATEGY FOR DMM SUPERCELL

This section systematically investigates the defect cavity configuration for enhancing sensing signal performance through the analysis of the complete band structure of the DMM functional unit. This involves a detailed investigation of defect bands responsible for energy localization and confinement in the dual defect DMM supercell.

2.1 Functional unit design of DMM

The DMM functional unit was engineered to achieve a complete bandgap through an integrated waveguide design, as illustrated in Figure 1(a). The configuration comprises a steel cylindrical stub bonded to a 2-mm-thick aluminum host plate, with perfect interfacial adhesion assumed to prevent delamination. Dispersion relations were calculated using a finite element model (FEM) with Bloch-Floquet boundary conditions in COMSOL Multiphysics® version 6.1 (Figure 1(b)), enabling comprehensive analysis of elastic wave propagation within the metamaterial structure. The irreducible Brillouin zone emphasizing the primitive vectors of the square lattice is presented in Figure 1(c), with detailed geometric parameters and material properties cataloged in Table 1.

Figure 1(d) displays the calculated all-polarized band structure of the unit cell, revealing a complete bandgap spanning 125.04-145.42 kHz – critical for defect mode formation. This frequency range aligns with operational requirements for nonlinear ultrasonic crack detection in thin-plate structures, where both symmetric (S0) and antisymmetric (A0) Lamb wave modes demonstrate significant propagation characteristics. Particular emphasis is placed on the fundamental A0 mode due to its enhanced crack sensitivity from shorter wavelengths compared to S0 modes, characterized by out-of-plane displacement along propagation paths.

To differentiate various polarized modes, the polarization amount P_z for out-of-plane wavefield is quantified as follows:

$$P_Z = \frac{\int_{V_{plate}} |u_z|^2 \, dV}{\int_{V_{plate}} \left(\int_{V_{plate}} |u_x|^2 + |u_y|^2 + |u_z|^2 \right) dV} \tag{1}$$

In this equation, u_x, u_y, and u_z denote displacements in the x, y, and z directions, respectively.

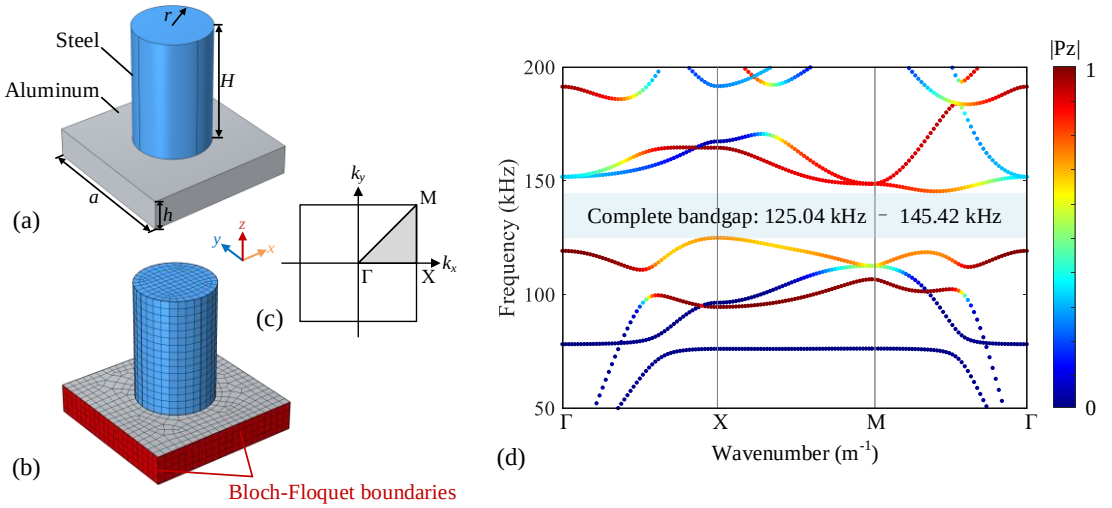

Figure 1. (a) Schematic representation of the proposed DMM functional unit. (b) Finite element model employed for deriving dispersion curves of the metamaterial system. (c) Illustration of the irreducible Brillouin zone, highlighting the primitive vectors within a square lattice. (d) Band structure of the DMM functional unit along the irreducible Brillouin zone path (Γ-X-M-Γ) in the square lattice.

Table 1. Geometric parameters and material properties of corresponding components and materials in numerical modeling.

Geometric Parameter	Value (*mm*)	Material Property	Value
Lattice constant, *a*	10	Density of Aluminum	2700 kg/m^3
Thickness of aluminum plate, *h*	2	Young's modulus of Aluminum	70 *GPa*
Radius of steel stub, *r*	2.5	Poisson's ratio of Aluminum	0.33
Height of steel stub, *H*	8	Density of Steel	7760 kg/m^3
Length of T-PWAS	10	Young's modulus of Steel	220 *GPa*
Width of T-PWAS	50	Poisson's ratio of Steel	0.30
Radius of R-PWAS	2.5	Density of PWAS	7600 kg/m^3
Height of PWAS	0.2		

2.2 Defect band characteristics in supercell configuration

To investigate wave localization in a system with broken periodicity, a 7 × 5 supercell configuration composed of identical unit cells was employed. This arrangement incorporated a two-point defect mode, as depicted in Figure 2(a) and (b), where steel rods were removed from the 3rd and 4th layers to create a defect cavity. Strategic removal of steel rods addresses two competing considerations[28]: (1) the requirement for an adequate number of unit cells surrounding the defect to facilitate bandgap formation, and (2) the benefit of positioning the defect cavity near the first layer to amplify the evanescent wave amplitude. Unlike the bandgap analysis performed at the unit cell scale, the defect band analysis was conducted using supercell calculations. The irreducible Brillouin zone, defined by the primitive vectors of the rectangular lattice, is presented in Figure 2(c). The resulting band structure, shown in Figure 2(d), reveals six defect bands within the complete bandgap range. Among these, four prominent defect bands—designated as Defect modes A to D—exhibit significant out-of-plane polarization at frequencies of 127.34 kHz, 130.63 kHz, 135.56 kHz, and 138.59 kHz, respectively. Their flat dispersion relations suggest efficient elastic wave confinement – a consequence of the "wall

effect" where surrounding cells impose fixed boundary conditions, inducing mechanical resonance and evanescent wave localization.

To assess the potential of these defect modes for wave localization and energy enhancement, the eigenmode shapes of the defect modes were examined. As illustrated in Figure 2(e)-(h), four distinct wave localization patterns are identified. Each defect mode exhibits a unique displacement field confined within the defect cavity. Notably, a monopole-like defect mode shape, shown in Figure 2(g), corresponds to the transverse polarization displacement field (i.e., out-of-plane mode shape). This mode effectively localizes the A0 Lamb mode and enhances the concentration of wave energy. These findings suggest that the two-point defect mode supercell configuration is well-suited for further exploration in wave localization studies.

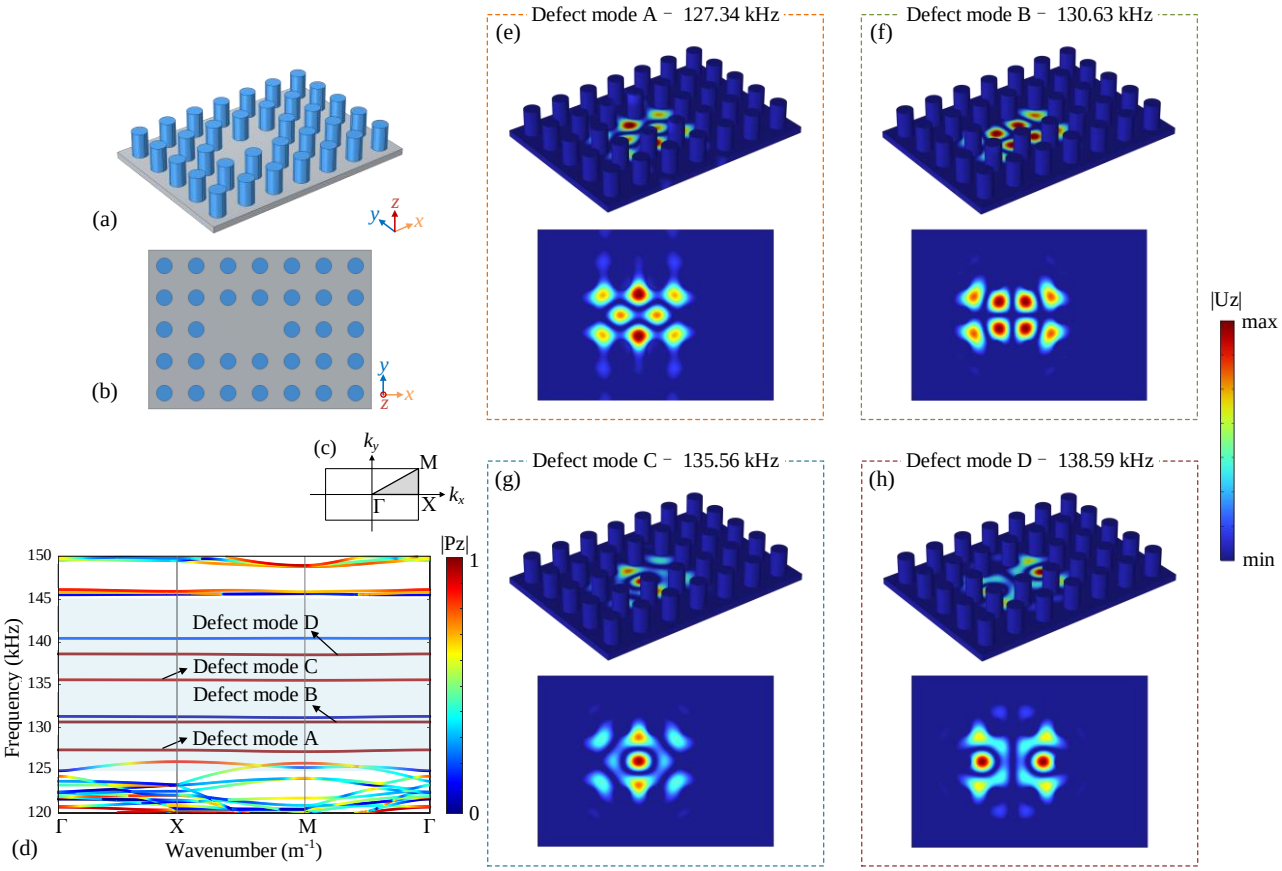

Figure 2. (a) Three-dimensional (3D) representation and (b) top view of the two-point defect mode supercell configuration. (c) Illustration of the irreducible Brillouin zone with primitive vectors within a rectangle lattice. (d) The corresponding band structure and polarization magnitude of the supercell configuration, highlighting four defect modes: A, B, C, and D. The absolute displacement field (U_Z) distribution for (e) Defect mode A (127.34 kHz), (f) Defect mode B (130.63 kHz), (g) Defect mode C (135.56 kHz), and (f) Defect mode D (138.59 kHz), as indicated in (d).

3. NUMERICAL DEMONSTRATION OF WEAK NONLINEAR FEATURE AMPLIFICATION

This section examines the spectral responses of both the DMM and smooth plates, with a focus on identifying optimal excitation frequencies that maximize signal enhancement at the sensing end. Transient dynamic analyses were conducted to elucidate the signal enhancement mechanism attributed to the nonlinear characteristics induced by fatigue cracks. These findings underscore the system's capability to detect and amplify subtle nonlinear features associated with structural damage.

3.1 Model configuration for DMM system

The numerical model configuration of the DMM plate, as illustrated in Figure 3(a), was established to conduct harmonic analysis and derive frequency spectral responses. A square transmitter PWAS (T-PWAS), with dimensions of 10 mm × 5 mm × 0.2 mm, was positioned 100 mm from the left boundary of the DMM region to generate incident waves propagating in the A0 and S0 modes along the positive *x*-direction. To minimize boundary reflections, non-reflective boundaries (NRBs) were implemented at both ends of the structure. Additionally, periodic boundary conditions (PBCs) were applied along the lateral boundaries to simulate two-dimensional wave propagation in an extensive plate, while the remaining surfaces were left unconstrained. A circular receiver PWAS (R-PWAS), with a radius of 5 mm and a thickness of 0.2 mm, was strategically positioned at the center of the defect cavity, symmetrically aligned across the *y*-axis within the DMM region. A voltage of 100 peak-to-peak (vpp) was applied to the top surface of the T-PWAS, with the bottom surface grounded. Similarly, the top surface of the R-PWAS served as the positive electrode for sensing signal acquisition, while the bottom surface was grounded. Both the T-PWAS and R-PWAS were assigned the material properties of APC-850 as follows:

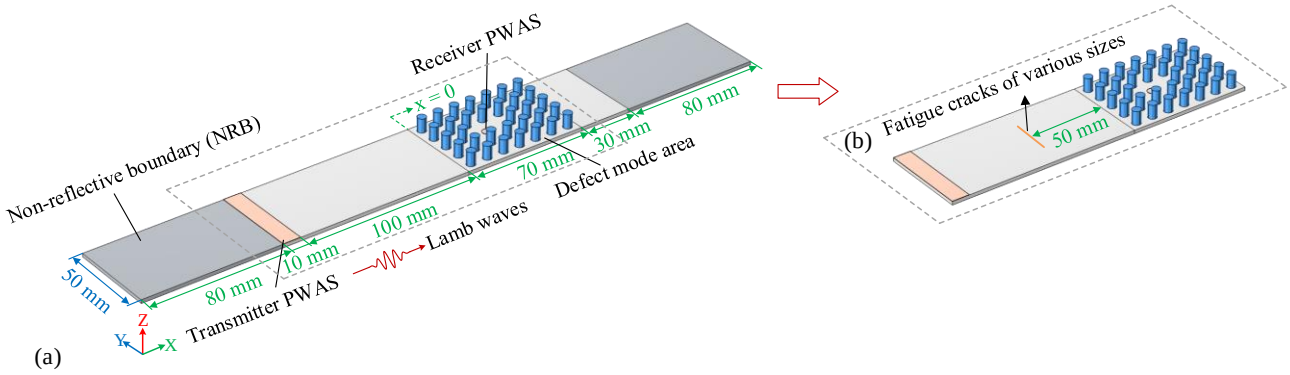

Figure 3. Numerical model configuration illustrating the two-point defect mode distribution of the metamaterial units for harmonic and transient analyses: (a) general model setup and (b) detailed zoom-in view of the fatigue crack implemented between the DMM array and the T-PWAS.

$$\left[C_p\right]=\begin{bmatrix} C_{11} & & & & & \\ C_{21} & C_{22} & & & & \\ C_{31} & C_{32} & C_{33} & & & \\ C_{41} & C_{42} & C_{43} & C_{44} & & \\ C_{51} & C_{52} & C_{53} & C_{54} & C_{55} & \\ C_{61} & C_{62} & C_{63} & C_{64} & C_{65} & C_{66} \end{bmatrix}=\begin{bmatrix} 97 & 44 & 49 & 0 & 0 & 0 \\ 44 & 97 & 49 & 0 & 0 & 0 \\ 49 & 49 & 84 & 0 & 0 & 0 \\ 0 & 0 & 0 & 22 & 0 & 0 \\ 0 & 0 & 0 & 0 & 22 & 0 \\ 0 & 0 & 0 & 0 & 0 & 26.5 \end{bmatrix} GPa \tag{2}$$

$$\left[\varepsilon_p\right]=\begin{bmatrix} \varepsilon_{11} & & \\ & \varepsilon_{22} & \\ & & \varepsilon_{33} \end{bmatrix}=\begin{bmatrix} 947 & 0 & 0 \\ 0 & 947 & 0 \\ 0 & 0 & 605 \end{bmatrix}\times 10^{-8}\, F\cdot m^{-1} \tag{3}$$

$$\left[e_p\right]=\begin{bmatrix} e_{11} & e_{21} & e_{31} & e_{41} & e_{51} & e_{61} \\ e_{12} & e_{22} & e_{32} & e_{42} & e_{52} & e_{62} \\ e_{13} & e_{23} & e_{33} & e_{43} & e_{53} & e_{63} \end{bmatrix}=\begin{bmatrix} 0 & 0 & 0 & 0 & 12.84 & 0 \\ 0 & 0 & 0 & 12.84 & 0 & 0 \\ -6.02 & -6.02 & 22.31 & 0 & 0 & 0 \end{bmatrix} C\cdot m^{-2} \tag{4}$$

where $[C_p]$ represents the stiffness matrix, $[\varepsilon_p]$ is the dielectric matrix, and $[e_p]$ denotes the piezoelectric matrix.

3.2 Spectral responses of the DMM and smooth plate systems

To investigate the tuning effect induced by the structural dimensions of the system and to highlight the enhancement of sensing signals associated with defect bands, a comparative analysis of the harmonic responses between the DMM plate and a smooth plate without the DMM region was conducted, as shown in Figure 4(a). The frequency spectra reveal

significant differences between the two systems, with the DMM plate exhibiting four distinct peaks at 125.92 kHz, 130.32 kHz, 137.8 kHz, and 147.96 kHz. At these frequencies, the R-PWAS consistently records a substantial increase in sensing signal energy. In contrast, the smooth plate, as depicted in Figure 4(b), displayed no comparable phenomenon. To further quantify the amplification effect of the sensing signals, a normalization procedure was employed. This approach resulted in a vertical axis representing a magnitude ratio coefficient, which quantifies the enhancement of ultrasonic guided waves within the DMM system, as described by the following equation:

$$Magnitude\ Ratio = V_{DMM} / V_{SP} \tag{5}$$

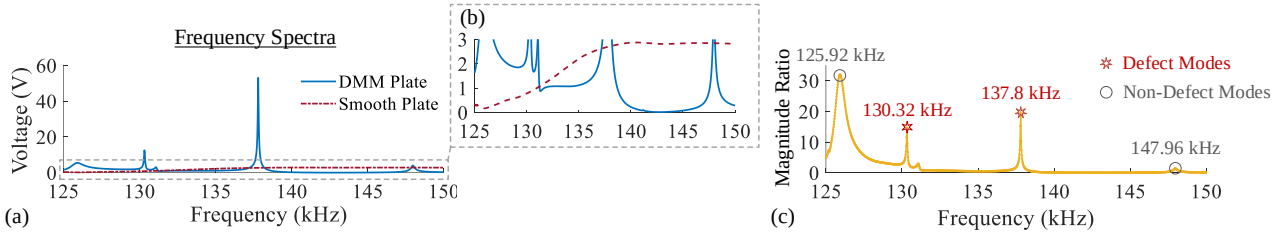

Figure 4. (a) Frequency spectra of sensing signals from the R-PWAS for DMM and smooth plates. (b) Detailed zoom-in view of the frequency spectra. (c) Comparison of harmonic responses showcasing four excitation frequencies identified as defect modes at 130.32 kHz and 137.8 kHz and non-defect modes at 125.92 kHz and 147.96 kHz.

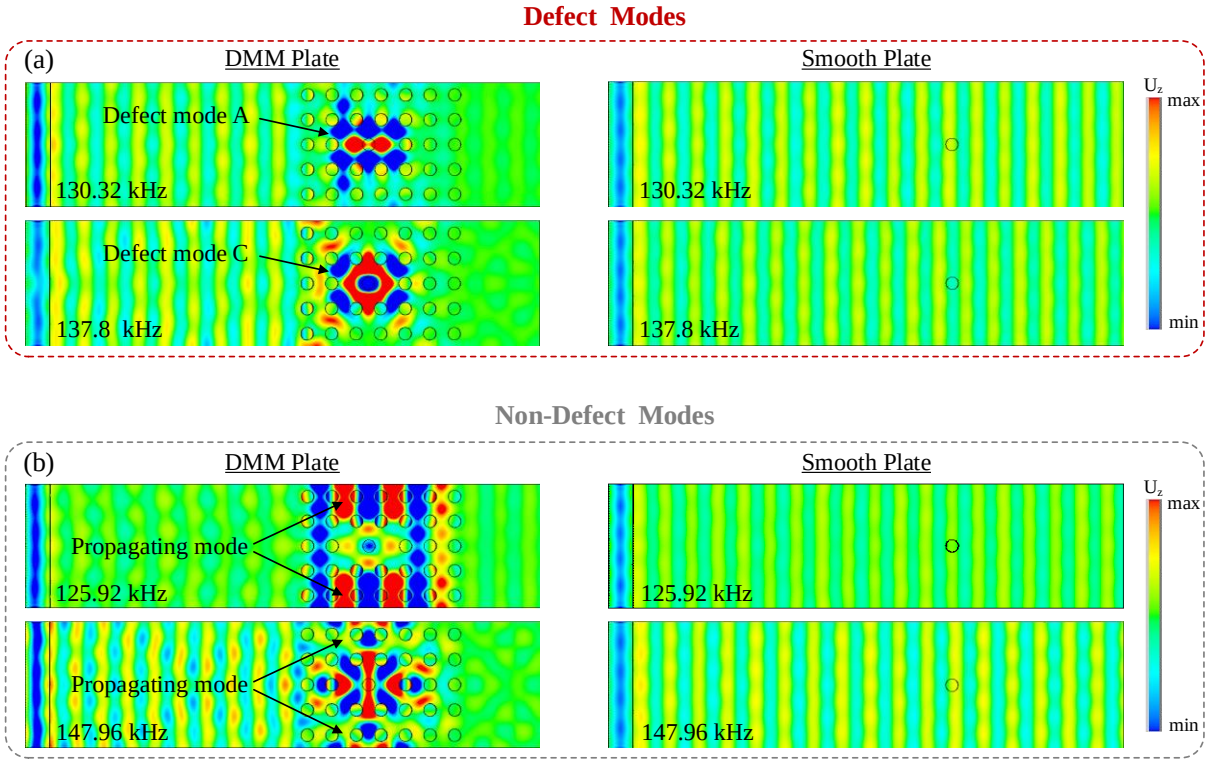

Figure 5. The out-of-plane displacement wavefields for the DMM plate and a smooth plate measured at excitation frequencies representing (a) defect modes and (b) non-defect modes.

As illustrated in Figure 4(c), the spectral profile exhibits pronounced sharpness in the vicinity of 130.32 kHz and 137.8 kHz, signifying a marked enhancement in sensing response as the excitation frequency converges toward these specific values. This behavior is ascribed to wave confinement phenomena linked to the defect band. Simultaneously, the magnitude ratio attains its peak at 125.92 kHz, a feature that contrasts with the absolute voltage response. This divergence is elucidated by Figure 4(b), which reveals a local minimum in the sensing signal amplitude slightly above 125 kHz, thereby causing the corresponding magnitude ratio to achieve a local maximum. A comparable trend is

observed at 147.96 kHz, where a gradual increase is noted, although this pattern does not conclusively indicate an influence from the defect band.

Figure 5 presents the out-of-plane displacement wavefields for both DMM and smooth plates at four characteristic excitation frequencies, further substantiating the previously discussed phenomena. As demonstrated in Figure 5(a), at 130.32 kHz and 137.8 kHz, distinct wave localization and confinement effects are prominently observed within the DMM plate. These wavefield distributions align with Defect mode A and Defect mode C, as identified in the modal analysis depicted in Figure 2(e) and (g), respectively. Consistent with prior observations, at 125.92 kHz and 147.96 kHz (Figure 5(b)), the DMM region exhibits two distinct propagating modes. Guided waves propagate along the waveguide, highlighting the ability of the R-PWAS to detect sensing signals in these scenarios, albeit with significantly reduced response amplitudes compared to those under defect mode conditions. In contrast, the smooth plates do not exhibit these phenomena, with guided waves propagating as planar waves along the waveguide.

For Defect modes A and C, the frequencies identified through modal and harmonic analyses display discrepancies. This can be explained by the fact that in harmonic analysis, the functional units are distributed over a finite length along the wave propagation direction (*x*-axis), differing from the assumptions inherent in modal analysis. Variations in peak frequencies corresponding to maximum wave energy confinement along the *x*-axis are attributed to differences in unit cell distribution. A sufficient number of unit cells is crucial for the emergence of bandgap characteristics or energy localization within the defect cavity. The slight shifts in peak frequencies are directly influenced by these variations, affecting wave propagation and energy confinement patterns within the DMM structure.

3.3 Transient dynamic analyses of the DMM and smooth plate systems with fatigue cracks

Harmonic analysis of the frequency spectra, as discussed in the preceding section, identifies 137.8 kHz as the frequency at which the ultrasonic guided wave within the DMM plate achieves optimal wave energy confinement, thereby significantly enhancing the sensing signal. Consequently, 137.8 kHz is selected as the target frequency for second harmonic enhancement in subsequent investigations. A 100 vpp, 20-count Hanning-window modulated sine tone burst signal, centered at 68.9 kHz, was applied to the top electrode of the T-PWAS. The simulation followed the standardized model configuration illustrated in Figure 3(b). An idealized "breathing crack" was introduced between the T-PWAS and the DMM region, positioned 50 mm from the T-PWAS and symmetrically aligned along the *y*-axis, perpendicular to the wave propagation direction (*x*-axis). The "breathing crack" model serves as a nonlinear source to represent localized damage, capturing the essential nonlinear characteristics of fatigue cracks, despite not precisely replicating real-world crack conditions. The crack's open/close behavior was determined based on the tension and compression states of a thin layer of nonlinear contact elements simulating CAN.

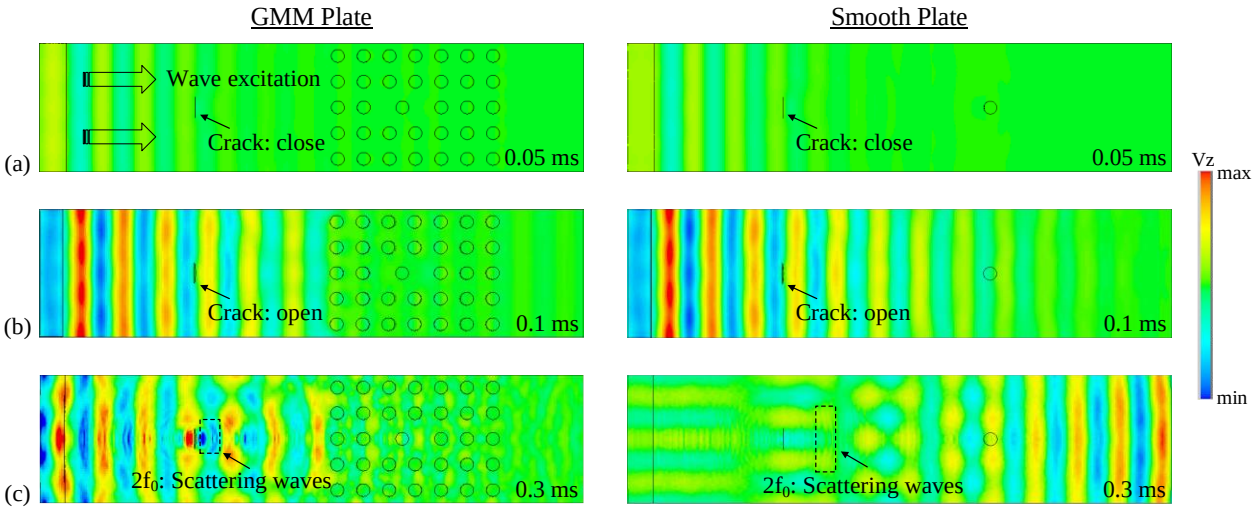

Figure 6. The snapshots of the out-of-plane velocity wavefields for the DMM and smooth plates with a breathing crack measured at different time steps: (a) 0.05 ms, (b) 0.1 ms, and (c) 0.3 ms.

The crack size was systematically increased from 2 mm to 10 mm in 2 mm increments. Figure 6 depicts the generation of the A0 wave mode and its interaction with a through-thickness breathing crack during the opening and closing processes.

Snapshots of out-of-plane velocity wave propagation capture the generation, propagation, and scattering of the A0 wave at the fatigue crack. The primary wave front exhibits shading due to interference with the scattered wave field, which comprises multiple wave components with varying wavelengths and group velocities. These components likely arise from higher harmonic modes of the same wave or converted wave modes. The nonlinearity in wave-crack interactions results from periodic changes in local stiffness during the crack's dynamic opening (Figure 6(b)) and closing (Figure 6(c)) processes.

Figure 7 presents the temporal signals recorded by the R-PWAS, along with the corresponding frequency spectra obtained via Fast Fourier Transform (FFT) analysis. Examination of the R-PWAS time traces reveals that as the crack size increases from 2 mm to 10 mm, the temporal domain of the GMM displays an increasing number of zigzag patterns, primarily localized around the primary wave packet of the fundamental frequency. This trend indicates a progressive intensification of nonlinear characteristics, a phenomenon absents in the smooth plate configuration. Comparative analysis of the frequency spectra for the two plate types reveals distinct differences. Notably, the fundamental frequency magnitude is significantly reduced due to the DMM effect, while the second harmonic magnitude is markedly amplified, consistent with the temporal response characteristics.

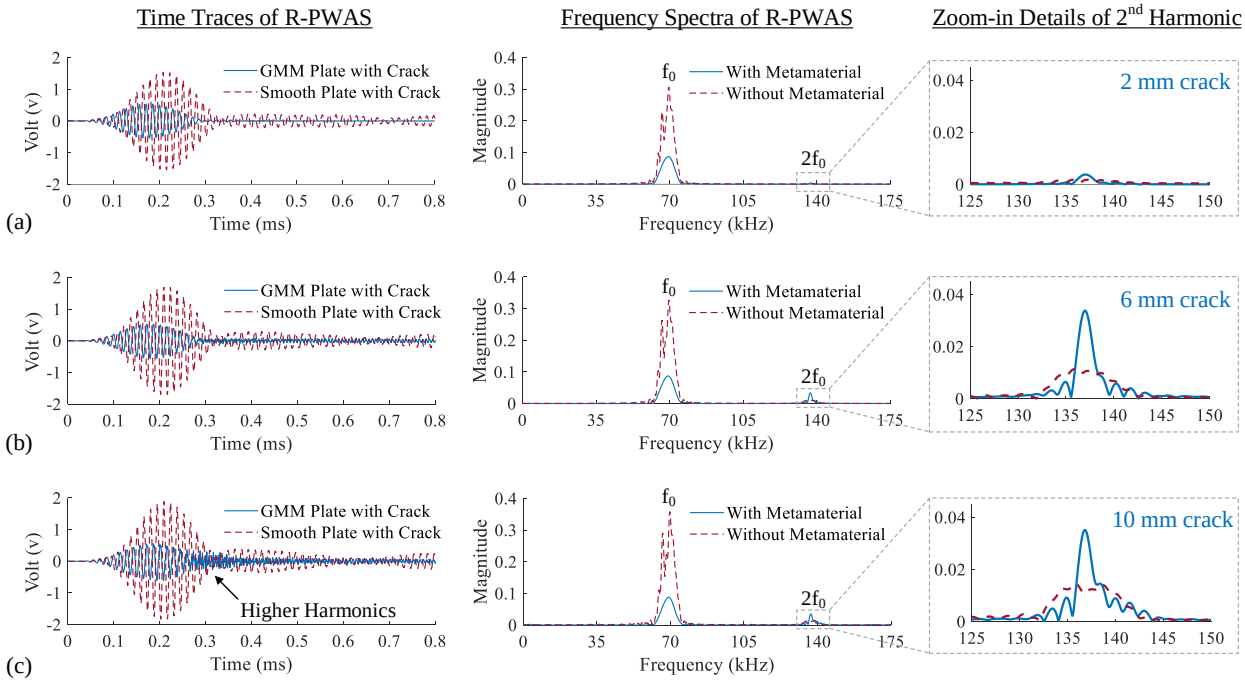

Figure 7. Exemplary time traces and frequency spectra of the sensing signals, along with zoom-in details of the second harmonic for GMM and smooth plates under different crack conditions: (a) 2-mm, (b) 6-mm, and (c) 10-mm breathing crack.

To further elucidate these differences, Figure 8(a) illustrates the absolute magnitude of the second harmonic for both the DMM and smooth plates, as well as the magnitude ratio of the second harmonic between the two configurations. The results demonstrate that the absolute magnitude of the $2f_0$ component increases monotonically with crack size for both configurations. However, the rate of increase is significantly higher for the DMM plate, indicating greater sensitivity to fatigue crack size enlargement. The magnitude ratio parameter reveals that the DMM effect enhances the second harmonic by up to 3.33 times for an 8-mm crack. Even for smaller cracks, such as 2 mm, the enhancement reaches 2.16 times, substantially improving the detection sensitivity of nonlinear ultrasonic techniques for fatigue cracks. Figure 8(b) shows the magnitude ratio between the second harmonic and the fundamental frequency for both DMM and smooth plates. The results indicate that the DMM configuration significantly increases the proportion of $2f_0$ relative to f_0 compared to the smooth plate, with this ratio also rising substantially with crack size enlargement. This suggests that the DMM not only amplifies subtle second harmonic features for fatigue crack detection but also effectively filters out the fundamental signal, which is unrelated to fatigue crack detection, thereby rendering nonlinear characteristics more pronounced.

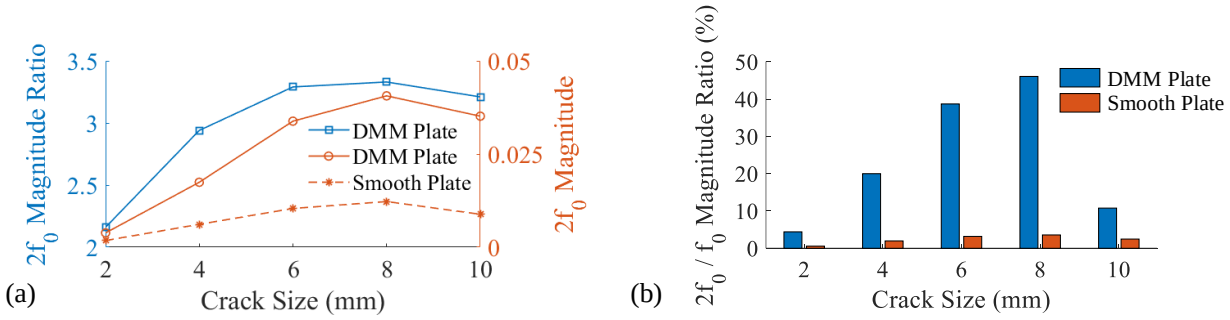

Figure 8. (a) The absolute magnitude of second harmonic for DMM and smooth plates (*y*-axis on the right) and the magnitude ratio of second harmonic between these two scenarios (*y*-axis on the left). (b) The magnitude ratio between the second harmonic and the fundamental frequency for both DMM and smooth plates.

4. CONCLUDING REMARKS

An elastic defect mode metamaterial (DMM) was developed to significantly enhance sensitivity in the detection of fatigue cracks. The DMM incorporates a two-point defect cavity, characterized by a specific monopole defect mode that amplifies the sensing signal captured by a received piezoelectric wafer active sensor (R-PWAS). The study highlights the efficacy of the elastic DMM in addressing the challenges associated with detecting subtle nonlinear characteristics during the early stages of fatigue crack nucleation and growth. Through numerical simulations, supported by harmonic and transient dynamic analyses, the research demonstrates the capability of DMM to improve the detection of the second harmonic generated by contact acoustic nonlinearity (CAN) arising from wave-crack interactions. These findings underscore the potential of the proposed elastic metamaterial framework to enhance fatigue crack detection sensitivity, offering promising implications for future applications in Structural Health Monitoring (SHM) and Nondestructive Evaluation (NDE).

In terms of prospective investigations, the utilization of Scanning Laser Doppler Vibrometry is recommended to experimentally assess the wave energy confinement phenomenon facilitated by the proposed DMM. Ongoing efforts are underway, with the anticipation of key results to be disseminated in an upcoming journal publication.

5. ACKNOWLEDGEMENTS

The support from the National Natural Science Foundation of China (contract number 52475161) and the China Postdoctoral Science Foundation (contract number 2024M761957) are thankfully acknowledged. Dr. Yanfeng Shen appreciates the funding from John Wu & Jane Sun Endowed Professorship.

REFERENCES

[1] Jhang K-Y. Nonlinear ultrasonic techniques for nondestructive assessment of micro damage in material: a review. International Journal of Precision Engineering and Manufacturing 2009;10:123-35.
[2] Yun H, Rayhana R, Pant S, Genest M, and Liu Z. Nonlinear ultrasonic testing and data analytics for damage characterization: A review. Measurement 2021;186:110155.
[3] Xu L, Wang K, Yang X, Su Y, Yang J, Liao Y, Zhou P, and Su Z. Model-driven fatigue crack characterization and growth prediction: A two-step, 3-D fatigue damage modeling framework for structural health monitoring. International Journal of Mechanical Sciences 2021;195:106226.
[4] Andreades C, Malfense Fierro GP, and Meo M. A nonlinear ultrasonic modulation approach for the detection and localisation of contact defects. Mechanical Systems and Signal Processing 2022;162:108088.
[5] Lu R, Shen Y, Zhang B, and Xu W. Nonlinear Electro-Mechanical Impedance Spectroscopy for fatigue crack monitoring. Mechanical Systems and Signal Processing 2023;184:109749.

[6] Lim HJ, Sohn H, DeSimio MP, and Brown K. Reference-free fatigue crack detection using nonlinear ultrasonic modulation under various temperature and loading conditions. Mechanical Systems and Signal Processing 2014;45:468-78.
[7] Hanuman NSVN, Roy S, and Bose T. Detection of local defect resonance intermodulation peaks using bicoherence analysis. International Journal of Mechanical Sciences 2019;163:105092.
[8] Gao M, Feng Y, Hu X, Ng CT, and Kotousov A. Delamination detection in composite pipes using higher harmonic generation of flexural waves. Composite Structures 2024;346:118418.
[9] Lu R and Shen Y. Entire loosening stage monitoring of bolted joints via nonlinear electro-mechanical impedance spectroscopy. Structural Health Monitoring 2024.
[10] Yang H, Yang Z, Lu S, Shan Y, Ma J, Yang L, and Wu Z. Ultrasonic imaging of delamination in thick CFRP laminates using an energy-compensation reverse time migration method. Ultrasonics 2024;138:107253.
[11] Bermes C, Kim J-Y, Qu J, and Jacobs LJ. Experimental characterization of material nonlinearity using Lamb waves. Applied Physics Letters 2007;90:021901.
[12] Sampath S and Sohn H. Detection and localization of fatigue crack using nonlinear ultrasonic three-wave mixing technique. International Journal of Fatigue 2022;155:106582.
[13] Lim HJ, Song B, Park B, and Sohn H. Noncontact fatigue crack visualization using nonlinear ultrasonic modulation. NDT & E International 2015;73:8-14.
[14] Wang Z, Zhang S, Li Y, Wang Q, Su Z, and Yue D. A Cross-Scanning Crack Damage Quantitative Monitoring and Imaging Method. IEEE Transactions on Instrumentation and Measurement 2022;71:1-10.
[15] Chen YY, Zhu R, Barnhart MV, and Huang GL. Enhanced flexural wave sensing by adaptive gradient-index metamaterials. Scientific Reports 2016;6:35048.
[16] Liu Z, Zhang X, Mao Y, Zhu YY, Yang Z, Chan CT, and Sheng P. Locally resonant sonic materials. Science 2000;289:1734-36.
[17] Cao L, Yang Z, Xu Y, Chen Z, Zhu Y, Fan S-W, Donda K, Vincent B, and Assouar B. Pillared elastic metasurface with constructive interference for flexural wave manipulation. Mechanical Systems and Signal Processing 2021;146:107035.
[18] Zhu R, Liu XN, Hu GK, Sun CT, and Huang GL. Negative refraction of elastic waves at the deep-subwavelength scale in a single-phase metamaterial. Nature Communications 2014;5:5510.c
[19] Tian Y, Shen Y, Rao D, and Xu W. Metamaterial improved nonlinear ultrasonics for fatigue damage detection. Smart Materials and Structures 2019;28:075038.
[20] Zhang X, Zhang J, Xu C, Rong J, Hu N, Deng M, and Zhang C. Inverse-designed flexural wave metamaterial beams with thermally induced tunability. International Journal of Mechanical Sciences 2024;267:109007.
[21] Chen Y, Liu H, Reilly M, Bae H, and Yu M. Enhanced acoustic sensing through wave compression and pressure amplification in anisotropic metamaterials. Nature Communications 2014;5:5247.
[22] Huang S, Lin Y, Tang W, Deng R, He Q, Gu F, and Ball AD. Sensing with sound enhanced acoustic metamaterials for fault diagnosis. Frontiers in Physics 2022;10:1027895.
[23] Xiao J, Ding X, Huang W, He Q, and Shao Y. Rotating machinery weak fault features enhancement via line-defect phononic crystal sensing. Mechanical Systems and Signal Processing 2024;220:111657.
[24] Zhang G-Y, Liu Z-J, Li B-Z, Dou X-L, Zhang C-R, Sun X-W, and Yang Y-M. Phononic crystals with incomplete line defects: applications in high-performance and broadband acoustic energy localization and harvesting. Smart Materials and Structures 2024;33:085036.
[25] Jo S-H and Youn BD. Longitudinal wave localization using a one-dimensional phononic crystal with differently patterned double defects. International Journal of Mechanical Sciences 2023;237:107783.
[26] Lee G, Park J, Choi W, Ji B, Kim M, and Rho J. Multiband elastic wave energy localization for highly amplified piezoelectric energy harvesting using trampoline metamaterials. Mechanical Systems and Signal Processing 2023;200:110593.
[27] Ma T-X, Fan Q-S, Li Z-Y, Zhang C, and Wang Y-S. Flexural wave energy harvesting by multi-mode elastic metamaterial cavities. Extreme Mechanics Letters 2020;41:101073.
[28] Jo S-H, Yoon H, Shin YC, Kim M, and Youn BD. Elastic wave localization and harvesting using double defect modes of a phononic crystal. Journal of Applied Physics 2020;127:164901.